ELSEVIER

Chemical Engineering Journal 85 (2002) 245–257

Chemical Engineering Journal

www.elsevier.com/locate/cej

Dynamics of non-isothermal adsorption in packed bed of biporous zeolites

Ivan Pentchev*, Kostadin Paev, Ilona Seikova

Department of Chemical Engineering, The University of Chemical Technology and Metallurgy, Blvd. Kliment Ohridski 8, Sofia 1756, Bulgaria

Received 5 December 1995; received in revised form 30 December 2000; accepted 28 March 2001

Abstract

Adsorption dynamics were investigated in a laboratory scale fixed bed column, functioning under three different non-isothermal conditions: adiabatic, near adiabatic and non-adiabatic. Axial and radial temperature profiles were registered, as well as a corresponding breakthrough curves at the column exit. Experimentally it has been demonstrated that the thermal effect of adsorption leads to deformation of the temperature profiles along the column. This directly affects the total amount adsorbed in the bed and breakthrough at the exit, an effect which is different for the different non-isothermal conditions. A two-dimensional mathematical model for description of non-isothermal adsorption was developed, including the effects of the radial temperature gradients. A biporous structure of the adsorbent particles is assumed and the heat effect on the equilibrium is taken into account. Good agreement is shown between experimental and theoretical results, when the mathematical model accounts for the radial thermal conduction and thermal flow through the wall.

Keywords: Gas adsorption; Fixed bed; Bidisperse adsorbent; Heat of adsorption; Non-isothermal; Numerical solution; Two-dimensional model

1. Introduction

It is well known that physical adsorption in packed beds is always coupled with some heat generation. In many cases this thermal effect has no significant influence on the adsorption dynamics and the process could be handled as an isothermal one. However, in practice, especially in treating high concentration feeds, the generated heat of adsorption leads to considerable temperature profiles in both radial and axial directions. These profiles change the equilibrium and transport characteristics depending on the heat amount emitted during the adsorption process.

This phenomenon reflects the mathematical modelling of the adsorption in packed beds and makes it quite difficult. The various models for non-isothermal adsorption differ in their generality concerning:

- operating mode (adiabatic or non-adiabatic with heat loss through the column walls);
- structure of the adsorbent solid matrix (single monodisperse pore structure or composite pellet with bidisperse pore distribution);
- flow structure in the bed (one- or two-dimensional).

Under these restrictions appropriate approximations are made concerning the effects of equilibrium, transfer resistances and axial dispersion on the overall process.

The first direct numerical solutions incorporating both equilibrium and kinetic effects were obtained by Carter [1] and by Meyer and Weber [2] for adiabatic adsorption. In these models the axial dispersion and external mass transfer around the adsorbent particles have been taken into account. The assumptions of adiabatic conditions are not rigorously fulfilled and the real behaviour of smaller units is non-adiabatic. The first study where the heat exchange through the walls has been considered, is proposed by Lee and Weber [3]. Similar one-dimensional model has been developed in the work of Ozil and Bonnetain [4] for a system in which the heat capacity of the fluid phase is negligible in comparison with the heat capacity of the adsorbent. Many other researches have derived both analytical and numerical solutions describing the dynamics of non-isothermal adsorption for different types of equilibrium isotherm [5–8].

The common deficiency in the above-cited models is the assumption of monodisperse pore structure within the adsorbent particle. To interpret accurately the transport phenomena in adsorbent with broad pore size distribution (such as activated carbon and zeolites), the real porous structure is idealised as a network of randomly interconnected pores with two distinct types of size: macro- and

* Corresponding author. Tel.: +359-2-62-54-643.

1385-8947/02/$ – see front matter
PII: S1385-8947(01)00160-7

Nomenclature

a_1	bed effective thermal dispersion coefficient ($m^2\,s^{-1}$)
A_0	pre-exponential multiplier
B_0	thermal coefficient
Bi^m	mass Biot number, $\beta R_2/D_1$
Bi^t	heat Biot number, $\alpha R_2/a_1$
C_1	sorbate concentration in the fluid phase ($kg\,m^{-3}$)
$C_{1,0}$	sorbate concentration in the fluid phase at the column inlet ($kg\,m^{-3}$)
C_2	sorbate concentration in the macroparticle ($kg\,m^{-3}$)
C_3	sorbate concentration in the microparticle ($kg\,m^{-3}$)
C_{eq}	sorbate equilibrium concentration ($kg\,m^{-3}$)
$\bar{C}$	volume averaged concentration ($kg\,m^{-3}$)
c_{p1}	heat capacity of the gas mixture ($J\,kg^{-1}\,K^{-1}$)
c_{p2}	heat capacity of the adsorbent ($J\,kg^{-1}\,K^{-1}$)
D_1	bed effective dispersion coefficient ($m^2\,s^{-1}$)
D_2	macropores effective diffusivity ($m^2\,s^{-1}$)
D_3	micropores effective diffusivity ($m^2\,s^{-1}$)
F_r	coefficient of Radke–Prausniz equilibrium ($m^{3N}\,kg^N$)
ΔH	heat of adsorption ($J\,kg^{-1}$)
K	external heat transfer coefficient ($W\,m^{-2}\,K^{-1}$)
K_r	coefficient of Radke–Prausniz equilibrium ($m^3\,kg^{-1}$)
L	column length (m)
$\bar{M}$	average molecular weight of the gas mixture ($kg\,kmol^{-1}$)
N_r	coefficient of Radke–Prausniz equilibrium
Nu	Nusselt number, $\alpha(2R_2)/\lambda_2$
Pe_1^m	bed mass Peclet number, V_1L/D_1
Pe_1^t	bed heat Peclet number, V_1L/a_1
Pe_2^m	macroparticle mass Peclet number, V_1R_2/D_2
Pe_2^t	particle heat Peclet number, V_1R_2/a_2
Pe_3^m	microparticle mass Peclet number, V_1R_3/D_3
R_1	column radius (m)
R_2	macroparticle radius (m)
R_3	microparticle radius (m)
R	universal gas constant ($J\,kg^{-1}\,K$)
Sh	Sherwood number, $\beta(2R_2)/D_2$
T_{amb}	ambient and initial fluid temperature (K)
$\bar{T}$	volume averaged temperature (K)
T_1	fluid temperature (K)
T_2	particle temperature (K)
q^*	equilibrium adsorption loading (g/g adsorbent)
q_a	adiabatic heat rise parameter, $(\Delta H/\rho_1 c_{p1})(C_{1,0}/T_{amb})$
q_w	heat loss parameter, KR_1/λ_1
x_1'	axial distance in the bed (m)
x_1''	radial distance in the bed (m)
x_2	radial distance in the macroparticle (m)
x_3	radial distance in the microparticle (m)
$Y_{1,0}$	initial mole fraction in the gas phase
V_1	fluid interstitial velocity ($m\,s^{-1}$)

Greek symbols

α	particle–fluid heat transfer coefficient ($W\,m^{-2}\,K^{-1}$)
β	particle–fluid mass transfer coefficient ($m\,s^{-1}$)
ε_1	void fraction in the bed
ε_2	void fraction in the macroparticle
λ_1	bed effective heat conductivity ($W\,m^{-1}\,K^{-1}$)
λ_2	particle effective heat conductivity ($W\,m^{-1}\,K^{-1}$)
ρ_1	gas mixture density ($kg\,m^{-3}$)
ρ_2	adsorbent particle density ($kg\,m^{-3}$)

Subscripts

1	gas phase
2	macroparticle
3	microparticle
eq	equilibrium

micropores. Existing models differ in the assumption of the dominating transport mechanism (most commonly is used pore or surface diffusion) and the coupling between diffusion/adsorption processes (parallel or consecutive) in macroporous and microporous structure. The first model taking into account simultaneous diffusion and adsorption in both macropores and micropores has been formulated and solved numerically by Ruckenstein et al. [9]. Many similar "parallel diffusion models" have been presented [10–15], where a parallel pore structure is assumed and local equilibrium is considered along the entire pore length. In the "consecutive diffusion models" a porous structure may be idealised as pores in series: micropores branching out from macropores, which themselves surround the microparticles. The macropores participate mostly in the transport of the solute (macropore diffusion). Adsorption occurs only on the microparticle surface, followed by diffusion in adsorbed state in a microporous structure within the microparticles (intracrystalline diffusion). In this case local equilibrium is established on the outer surface of the microparticle. Many researchers for adsorption process in zeolite [16–23] have used this type of models.

Most of the cited models neglect the radial temperature gradients and all resistance to heat transfer in radial direction is taken into account into an overall effective coefficient. More complex description of the fluid phase, considering two-dimensional mass and energy transport in packed bed is made by Kaguei et al. [24]. Farooq and Ruthven [25] made a comparison between one- and two-dimensional models,

assuming uniform particle temperature, negligible film resistance to heat transfer at the column wall, and linear adsorption equilibrium. The authors showed that one-dimensional model provides good results when the velocity of the concentration wave exceeds the thermal wave. Lin et al. [26] also compare the numerical solutions obtained from one- and two-dimensional model. It is shown that the effective overall coefficient of heat transfer is a very crucial parameter for one-dimensional analysis, as the agreement between the two models depends on the estimated values for this parameter.

Park and Knaebel [27] have studied experimentally and theoretically the adsorption of water vapour on silica gel. They showed that in case of complex isotherms of Type IV the heat effects could provoke unexpected shapes of the breakthrough curves. The experimental data, presented by the authors confirms the influence of the isothermal and non-isothermal conditions on the process dynamics.

The topic of the present paper is a comparative study of adsorption dynamic behaviour in different non-isothermal operation modes (adiabatic, near adiabatic and non-adiabatic). The experimental investigation includes measurements of axial and radial temperature profiles and respective concentration breakthrough curves. Two-dimensional model accounting for radial heat diffusion and thermal flow through the column wall is developed to interpret the dynamic behaviour of non-isothermal adsorption.

2. Experimental

2.1. Description of the experimental installation

The experimental set-up is shown in Fig. 1. It consists of fixed bed adsorption column (1) packed with Linde 4A zeolite adsorbent. Two different laboratory columns were used. The first one made of quartz is 30 cm long with inner diameter of 3 cm. The column was insulated with the vacuum jacket (10^{-4} mmHg). The second column has similar without vacuum insulation jacket. This column was also used with polystyrene insulation. An electrical heater (wire of 0.3 mm diameter) with power of 250 W was placed at the column axis. The heater was used for activation of the packed bed after the previous experiment.

The axial temperature profiles were measured by nine thermocouples (10), made by copper–constantan wires with diameter of 0.08 mm. These were located at a distance from the axis equal to half the column radius. The radial temperature profiles were recorded by other 10 thermocouples, situated at a uniform distance along the radius in the middle of the column.

The concentration of the gas mixture was registered by gas chromatography (6) with FID detector using an impulse sample injection device. Because of the high concentration of the gas sample a split injection technique (100:1) was used to take measurements in the linear response zone of the FID detector. A concentration calibration curve was also determined to ensure the proper detector response. The mean error of the concentration measurements was between 4 and 8%. The reference end of the thermocouples was cooled by data acquisition system HP 3421A-HP and then transferred to HP9000/332 workstation.

2.2. Operation mode

Before the beginning of each experiment the packed bed is activated by heating up to 400 °C for 3 h with continuous supply of argon (flow rate of 1.83×10^{-3} m^3 s^{-1}). After the thermal activation of the adsorbent the heating is stopped and the column is connected to the vacuum line until the bed reaches the ambient temperature.

After reaching the working temperature, the gas mixture with concentration controlled by gas chromatography passes

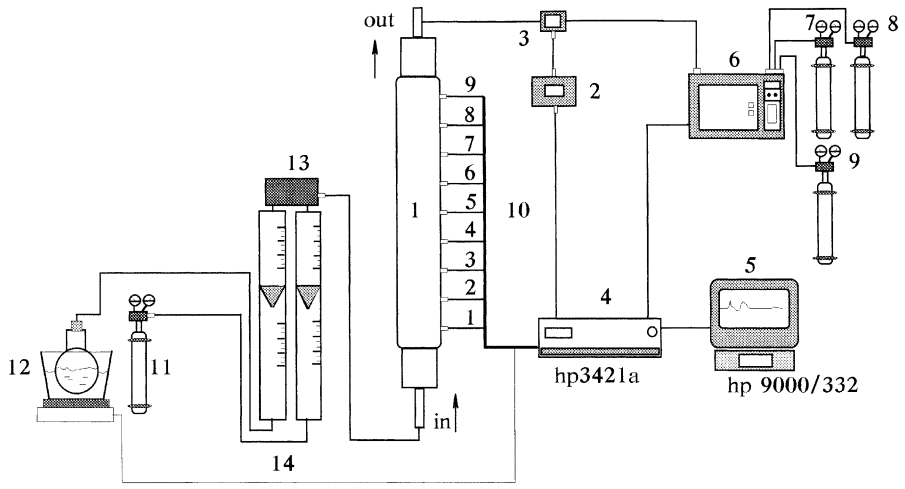

Fig. 1. Scheme of the experimental set-up. (1) Adsorption column; (2) control unit; (3) measuring valve; (4) data acquisition system; (5) computer; (6) gas chromatography; (7)–(9) gas supply; (10) thermocouples; (11) carrier gas supply; (12) vapour generator; (13) mixing chamber; (14) gas flow meters.

through the column. The gas mixture is composed of argon as inert carrier and water or acetone as absorbable component. During the experiment the concentration in the column inlet was kept constant using mass flow controller.

3. Modelling

The considered adsorber is a fixed bed column with constant void fraction ε_1 (Fig. 2). Gas mixture containing one absorbable component passes through the column at constant velocity V_1. The fixed bed represents an assembly of spherical particles with mean radius R_2. The adsorbent is considered as porous solid with bidisperse pore size distribution. The solid matrix of each particle is formed by uniformly distributed small microporous spheres characterised by mean radius R_3. Macropores are formed in the space among microparticles. The macropore volume forms the void fraction of the macroparticles ε_2. Macropore size of Linde 4A zeolite is in order of magnitude of 10^{-4} to 10^{-6} m and their contribution to the total active adsorption surface is negligible in respect to the microparticle surface.

The adsorption process occurs in several steps: (1) transfer of the solute from the bulk stream to the external surface of the adsorbent; (2) transport through the macropores only by pore diffusion; (3) adsorption when the solute reaches the microparticle surface; (4) diffusion in adsorbed state in the micropore volume. Adsorption equilibrium is attained on the microparticle surface and the generated heat of adsorption is proportional to the equilibrium loading. The heat is removed from the particle into the surrounded fluid and then is carried away by the gas stream through the column. The process continues until the outlet concentration becomes equal to that of the inlet and the adsorbent is completely saturated with the absorbable component.

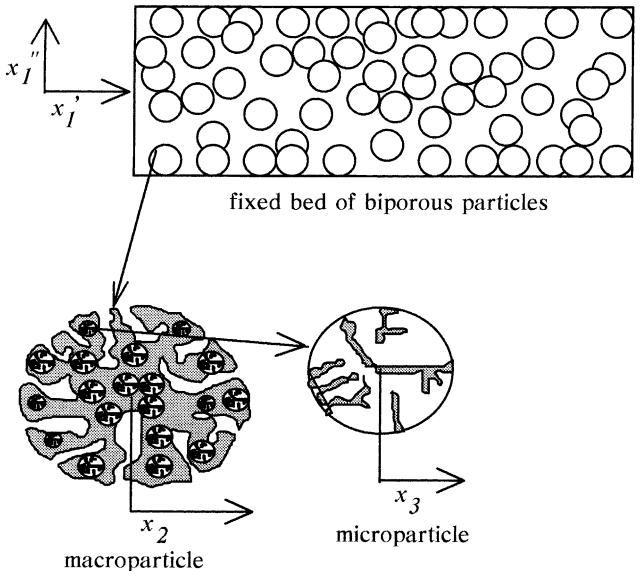

Fig. 2. Scheme of the packed bed with biporous particles.

The proposed mathematical model includes the following effects:

- diffusion through the fluid in both axial and radial directions;
- external mass transfer resistance around the adsorbent macroparticles;
- diffusion through the macropores;
- non-linear equilibrium on the microparticle surface; adsorption isotherm nearest to Type I is assumed and the appropriate experimental equilibrium data [28] is fitted by Radke–Prausnitz equation [29]

$$C_{\mathrm{eq}}(C_2, T) = \frac{K_{\mathrm{r}} C_2}{1 + (K_{\mathrm{r}}/F_{\mathrm{r}}) C_2^{N_{\mathrm{r}}-1}} \tag{1}$$

where the coefficients K_{r} and F_{r} are temperature dependent

$$K_{\mathrm{r}}(T) = A_0\, \mathrm{e}^{-\Delta H/RT} \text{ and } F_{\mathrm{r}}(T) = B_0\, \mathrm{e}^{-\Delta H/RT} \tag{2}$$

- diffusion in adsorbed state in micropore volume (intracrystalline diffusion);
- diffusion in both macropores and micropores can be described by Fick's equation; the effective diffusion coefficients are constant;
- generation of heat of adsorption;
- heat conduction inside the macroparticle: concerning the microparticles, the temperature gradients can be neglected due to the small sizes and high thermal conductivity of the zeolite crystals;
- external heat transfer resistance around the adsorbent macroparticles;
- heat diffusion through the fluid around the particles in axial and radial directions;
- heat exchange with the ambient space.

Three scales are necessary for describing mass and energy transfer processes at a different levels ($l = 1, 2, 3$):

1. axis symmetric cylindrical coordinates on the column level (axial x_1' and radial x_1'' coordinate);
2. centre symmetric spherical coordinates on the macroparticle level (x_2 coordinate);
3. centre symmetric spherical coordinates on the microparticle level (x_3 coordinate).

Under these assumptions the overall process in the fluid phase is described by the following set of mass and energy balance equations, including convective transport and both axial and radial dispersion.

Mass balance in the column:

$$\frac{\partial C_1(x_1', x_1'', t)}{\partial t} = -V_1 \nabla_{x_1'} C_1 + D_1 \nabla^2_{x_1'} C_1 + D_1 \nabla^2_{x_1''} C_1 - \frac{1-\varepsilon_1}{\varepsilon_1} \frac{\partial \bar{C}_2(x_1', x_1'', t)}{\partial t} \tag{3}$$

Energy balance in the column:

$$\frac{\partial T_1(x_1', x_1'', t)}{\partial t} = -V_1 \nabla_{x_1'} T_1 + a_1 \nabla^2_{x_1'} T_1 + a_1 \nabla^2_{x_1''} T_1 - \frac{1-\varepsilon_1}{\varepsilon_1(\rho_1 c_{p1})} \frac{\partial \bar{T}_2(x_1', x_1'', t)}{\partial t} \quad (4)$$

where $\bar{C}_2$ and $\bar{T}_2$ are the volume averaged concentration and temperature in the macroparticle and the last terms represent, respectively, the mass and energy flux per unit of volume, exchanged between the gas mixture and adsorbent phase.

Boundary conditions:

- At the column inlet section:

$$-D_1 \nabla_{x_1'} C_1(x_1', x_1'', t)|_{x_1'=0} = -V_1(C_{1,0} - C_1|_{x_1'=0}) \quad \text{for } 0 < x_1'' < R_1$$
$$-\lambda_1 \nabla_{x_1'} T_1(x_1', x_1'', t)|_{x_1'=0} = -V_1 \rho_1 c_{p1} - (T_{amb} - T_1|_{x_1'=0}) \quad \text{for } 0 < x_1'' < R_1 \quad (5)$$

- At the column outlet section:

$$\nabla_{x_1'} C_1(x_1', x_1'', t)|_{x_1'=L} = 0 \quad \text{for } 0 < x_1'' < R_1$$
$$\nabla_{x_1'} T_1(x_1', x_1'', t)|_{x_1'=L} = 0 \quad \text{for } 0 < x_1'' < R_1 \quad (6)$$

- At the column axis:

$$\nabla_{x_1''} C_1(x_1', x_1'', t)|_{x_1''=0} = 0 \quad \text{for } 0 \le x_1' \le L$$
$$\nabla_{x_1''} T_1(x_1', x_1'', t)|_{x_1''=0} = 0 \quad \text{for } 0 \le x_1' \le L \quad (7)$$

- On the column wall:

$$\nabla_{x_1''} C_1(x_1', x_1'', t)|_{x_1''=R_1} = 0 \quad \text{for } 0 \le x_1' \le L$$
$$-\lambda_1 \nabla_{x_1''} T_1(x_1', x_1'', t)|_{x_1''=R_1} = K(T_1|_{x_1''=R_1} - T_{amb}) \quad \text{for } 0 \le x_1' \le L \quad (8)$$

In the equations above the derivatives in axial and radial direction in cylindrical coordinates are noted as:

$$\nabla_{x_1'}(\cdot) = \frac{\partial(\cdot)}{\partial x_1'}; \qquad \nabla_{x_1''}(\cdot) = \frac{\partial(\cdot)}{\partial x_1''}; \qquad \nabla^2_{x_1'}(\cdot) = \frac{\partial^2(\cdot)}{\partial x_1'};$$
$$\nabla^2_{x_1''}(\cdot) = \frac{1}{x_1''} \frac{\partial}{\partial x_1''} \left(x_1'' \frac{\partial(\cdot)}{\partial x_1''} \right)$$

Macropores are considered only to transport mass and heat. The governing equations, including effective macropore diffusion, may be written as follows:

Mass balance in the macroparticle:

$$\frac{\partial C_2(x_1', x_1'', x_2, t)}{\partial t} = D_2 \nabla^2_{x_2} C_2 - \frac{1-\varepsilon_2}{\varepsilon_2} \frac{\partial \bar{C}_3(x_1', x_1'', x_2, t)}{\partial t} \quad (9)$$

Energy balance in the macroparticle:

$$(\rho_2 c_{p2}) \frac{\partial T_2(x_1', x_1'', x_2, t)}{\partial t} = \nabla_{x_2} \lambda_2(T_2) \nabla_{x_2} T_2 - \frac{1-\varepsilon_2}{\varepsilon_2} (\Delta H) \frac{\partial \bar{C}_3(x_1', x_1'', x_2, t)}{\partial t} \quad (10)$$

where $\bar{C}_3$ is the volume averaged concentration in the microparticle and the last terms represent, respectively, the mass flux per unit of volume, transferred toward the microparticles and the thermal flux of the generated heat of adsorption.

Boundary conditions:

- In the macroparticle centre:

$$\nabla_{x_2} C_2(x_1', x_1'', x_2, t)|_{x_2=0} = 0 \quad \text{for } \forall x_1', x_1''$$
$$\nabla_{x_2} T_2(x_1', x_1'', x_2, t)|_{x_2=0} = 0 \quad \text{for } \forall x_1', x_1'' \quad (11)$$

- On the macroparticle surface:

$$-D_2 \nabla T_2(x_1', x_1'', x_2, t)|_{x_2=R_2} = \beta(C_2|_{x_2=R_2} - C_1) \quad \text{for } \forall x_1', x_1''$$
$$\lambda_2(T_2) \nabla T_2(x_1', x_1'', x_2, t)|_{x_2=R_2} = \alpha(T_2|_{x_2=R_2} - T_1) \quad \text{for } \forall x_1', x_1'' \quad (12)$$

with the following notation for derivatives in radial direction in spherical coordinates:

$$\nabla_{x_2} = \frac{\partial(\cdot)}{\partial x_2}; \qquad \nabla_{x_2}(\nabla_{x_2}) = \nabla^2_{x_2} = \frac{1}{x_2^2} \frac{\partial}{\partial x_2} \left(x_2^2 \frac{\partial(\cdot)}{\partial x_2} \right)$$

Adsorption with non-linear equilibrium takes place on the microparticle surface. Effective mass diffusion and uniform temperature are considered within the microparticle volume.

A microparticle mass balance equation may be written in the form of

$$\frac{\partial C_3(x_1', x_1'', x_2, x_3, t)}{\partial t} = D_3 \nabla^2_{x_3} C_3 \quad (13)$$

Boundary conditions:

- In the microparticle centre:

$$\nabla C_3|_{x_3=0} = 0 \quad \text{for } \forall x_1', x_1'', x_2 \quad (14)$$

- On the microparticle surface:

$$C_3|_{x_3=R_3} = C_{eq}(C_2, T_2) \quad \text{for } \forall x_1', x_1'', x_2 \quad (15)$$

Table 1
Scale parameters in the set of dimensionless equations describing the non-isothermal adsorption

Convective	Diffusional in axial direction	Diffusional in radial direction	Mass and heat source terms
Level 1 (column bed)	$\frac{1}{Pe^{m}}$	$\frac{L}{R_1 Pe_1^{m}}$	$3\left(\frac{1-\varepsilon_1}{\varepsilon_1}\right)\left(\frac{Bi^{m}L}{Pe_2^{m}R_2}\right)$
	$\frac{1}{Pe^{t}}$	$\frac{L}{R_1 Pe_1^{t}}$	$3\left(\frac{1-\varepsilon_1}{\varepsilon_1}\right)\left(\frac{Bi^{t}L}{Pe_2^{t}R_2}\right)$
Level 2 (macroparticles)		$\frac{L}{R_2 Pe_2^{m}}$	$3\left(\frac{1-\varepsilon_2}{\varepsilon_2}\right)\left(\frac{Bi^{m}L}{Pe_2^{m}R_2}\right)$
		$\frac{L}{R_2 Pe_2^{t}}$	$\frac{\Delta H}{\rho_1 c_{p1}}\frac{C_{1,0}}{T_{amb}}$
Level 3 (microparticles)		$\frac{L}{R_3 Pe_3^{m}}$	

The derivatives in radial direction in the spherical microparticle are noted as:

$$\nabla_{x_3} C_3 = \frac{\partial C_3}{\partial x_3};$$

$$\nabla_{x_3} = (\nabla_{x_2} C_3) = \nabla_{x_3}^2 = \frac{1}{x_3^2}\frac{\partial}{\partial x_3}\left(x_3^2 \frac{\partial C_3}{\partial x_3}\right)$$

Under the proposed boundary conditions the following expressions may be given for the mean concentration and temperature variations:

- Between gas mixture and macroparticles:

$$\frac{\partial \bar{C}_2(x_1', x_1'', t)}{\partial t} = \frac{3\beta(C_2|_{x_2=R_2} - C_1)}{R_2},$$
$$\frac{\partial \bar{T}_2(x_1', x_1'', t)}{\partial t} = \frac{3\alpha(T_2|_{x_2=R_2} - T_1)}{R_2} \quad (16)$$

- Between macro- and microparticles:

$$\frac{\partial \bar{C}_3(x_1', x_1'', x_2, t)}{\partial t} = D_3 \nabla C_3|_{x_3=R_3} \quad (17)$$

The following initial conditions are applied to introduce the concentration step change at the inlet:

$$\begin{aligned} C_1 &= C_{1,0} && \text{for } \forall x_1'' \text{ and } x_1' = 0 \\ T_1 &= T_{amb} && \text{for } \forall x_1'' \text{ and } x_1' = 0 \\ C_2 &= 0 && \text{for } \forall x_1', x_1'' \text{ and } x_2 \\ T_2 &= T_{amb} && \text{for } \forall x_1', x_1'' \text{ and } x_2 \\ C_3 &= 0 && \text{for } \forall x_1', x_1'', x_2 \text{ and } x_3 \end{aligned} \quad (18)$$

The scale parameters in the dimensionless form of the Eqs. (3)–(17) are given in Table 1. The following dimensionless parameters were defined:

- bed mass and heat Peclet number: $Pe_1^{m} = (V_1 L/D_1)$; $Pe_1^{t} = (V_1 L/a_1)$;
- particle mass and heat Peclet number: $Pe_2^{m} = (V_1 R_2/D_2)$; $Pe_1^{t} = (V_1 R_2/a_2)$; $Pe_3^{m} = (V_1 R_3/D_3)$;
- mass and heat Biot number: $Bi^{m} = \beta R_2/D_1$; $Bi^{t} = \alpha R_2/a_1$;
- heat loss parameter: $q_w = (KR_1/\lambda_1)$;
- adiabatic heat rise parameter: $q_a = (\Delta H/\rho_1 c_{p1})(C_{1,0}/T_{amb})$.

The above described mathematical model was solved numerically by using the finite difference method. The second order equations were approximated by five-point fully implicit differential scheme. The alternate direction integration (ADI) method was used for the two-dimensional equations.

The experimental conditions employed in the adsorption measurements, the available values of the physical

Table 2
Summary of experimental conditions and estimated values of physical and transport parameters

$L = 0.3\,m$	$V_1 = 0.0432\,m\,s^{-1}$	
$\varepsilon_1 = 0.55$	$\varepsilon_2 = 0.34$	
$R_1 = 3 \times 10^{-2}\,m$	$R_2 = 0.75 \times 10^{-3}\,m$	$R_3 = 1 \times 10^{-6}\,m$
$D_1 = 3.4 \times 10^{-3}\,m^2\,s^{-1}$	$D_2 = 1.62 \times 10^{-5}\,m^2\,s^{-1}$	$D_3 R_3^{-2} = 2.94 \times 10^{-4}\,s^{-1}$
$\rho_1 c_{p1} = 0.934 \times 10^3\,J\,m^{-3}\,K^{-1}$		$(\rho_2 c_{p2}) = 0.957 \times 10^6\,J\,m^{-3}\,K^{-1}$
$K = 2.51\,W\,m^{-2}\,K^{-1}$ (polystyrene insulation)		$K = 8.62\,W\,m^{-2}\,K^{-1}$ (non-insulation)
$\lambda_1 = 0.2\,W\,m^{-1}\,K^{-1}$		$\lambda_2(T_2) = 12.5(1 + 4.5 \times 10^{-3} T_2^4)\,W\,m^{-1}\,K^{-1}$
$\alpha = 22.01\,W\,m^{-2}\,K^{-1}$	$\beta = 2.3 \times 10^{-5}\,m\,s^{-1}$	
Radke–Prausnitz equilibrium coefficients (Linde 4A, $T_{amb} = 20\,^{\circ}C$)		
Water: $K_r = 0.2156$	$N_r = 0.0456$	$F_r = 456$
Acetone: $K_r = 0.0987$	$N_r = 0.0345$	$F_r = 892.5$

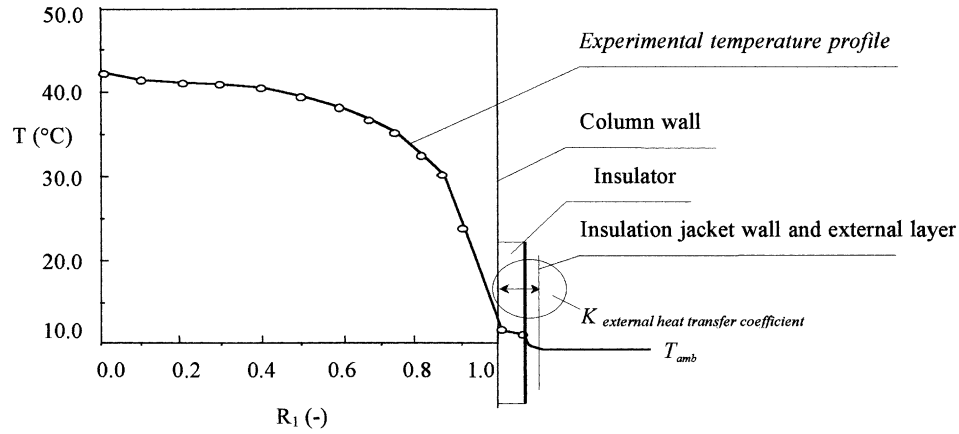

Fig. 3. Experimental determination of external heat transfer coefficient for non-adiabatic case.

characteristics and the estimated parameters used in the numerical study are listed in Table 2. Assuming analogy for the particle to fluid mass and heat transfer, the corresponding transfer coefficients were estimated from Wakao and Funazkri's correlations [30]:

$$Sh = \frac{\beta(2R_2)}{D_2} = 2.0 + 1.1\,Sc^{0.33}Re^{0.6}, \quad 3 < Re < 10^4$$
$$Nu = \frac{\alpha(2R_2)}{\lambda_2} = 2.0 + 1.1\,Pr^{0.33}Re^{0.6}, \quad 3 < Re < 10^4 \tag{19}$$

The same analogy is not applied to the mass and heat transfer coefficients in the bed. According to Wakao [31] effective thermal dispersion coefficient in the bed a_1 depends on the experimental conditions as follows:

$$a_1 = \frac{\lambda_1}{\varepsilon_1\rho_1 c_{p1}} + R_2 V_1 \tag{20}$$

The heat loss through the column walls in non-adiabatic conditions is taken into account by the external heat transfer coefficient. This coefficient is estimated experimentally on the basis of measured radial profiles (Fig. 3). The determination of the temperature gradient on the wall is then possible and the wall heat transfer coefficient is calculated from the boundary condition, Eq. (8) on the column wall:

$$K = \frac{-\lambda(\partial T_1/\partial x_1)|^{\exp}_{x_1=R_1}}{(T_1|^{\exp}_{x_1=R_1} - T_{\mathrm{amb}})} \tag{21}$$

Two extreme cases from near adiabatic and near-isothermal conditions may be easily derived from the more general non-adiabatic model:

- Adiabatic or near adiabatic conditions: in the boundary condition, Eq. (8), which expresses the heat loss through the column walls, the external heat transfer coefficient $K \approx 0$ may be used to simulate complete adiabatic process.
- Isothermal or near-isothermal conditions: the rise of the temperature as a result of heat of adsorption is neglected, which leads to the same temperature in the column and in the ambient space.

4. Experimental results

The temperature rises in axial as well as radial direction in the bed with the progress of adsorption. Typical experimental temperature profiles measured as a function of time along the column length are presented in Fig. 4 (vacuum insulation) and, respectively, in Fig. 5 (non-insulated column). The curves are recorded and numbered in accordance with the thermocouples positions. These experiments were performed using as influent argon–water gas mixture with superficial gas velocity of $V_1 = 0.0432\,\mathrm{m\,s^{-1}}$ and initial water vapour concentration $C_{1,0} = 2.37 \times 10^{-3}\,\mathrm{mol\,l^{-1}}$.

Three stages in the temperature profiles are observed. The rapid initial temperature increase (I stage) is followed by a low rise to the maximum value $T_{\max}$ (II stage) and gradually falling toward the initial temperature (III stage). At the beginning of the filling of the adsorption zone, the adsorbed amount increases very sharply and, as adsorption is exothermic, the temperature increases rapidly. The flat zone is a consequence of the fact that the quantity of the removed heat becomes of order of magnitude of the amount of carrier stream heat capacity, available to transport the heat away from the adsorption zone. In the third stage the heat transfer becomes more important than the heat generation: simultaneously with the decrease of the temperature the adsorption capacity increases but the approach to the equilibrium loading is very slow for an equilibrium isotherm of Type I.

The experimental profiles are similar to the curves obtained by Park and Knaebel [27], and by Vagliasindi and Hendrics [32]. Despite the heat loss through the column walls, the high value of the heat of adsorption of water on zeolites ($5660\,\mathrm{J\,mol^{-1}}$) provokes significant temperature

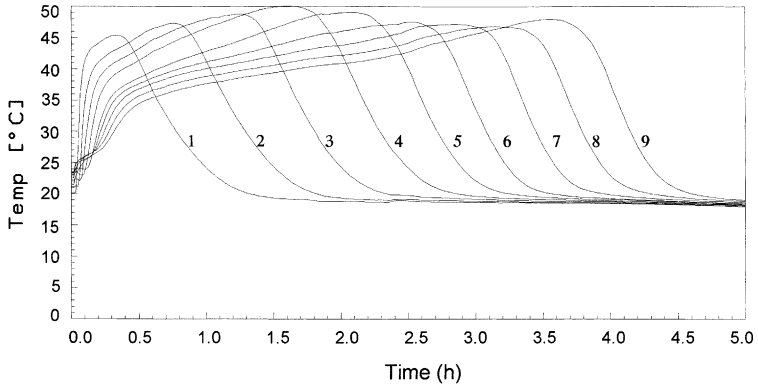

Fig. 4. Experimental temperature profiles measured by each thermocouple in time (adiabatic column: vacuum insulation, Water on Linde 4A zeolite, $V_1 = 0.0432\,\mathrm{m\,s^{-1}}$).

rise. As it is shown the highest peaks of the thermal waves are more than 30 °C for adiabatic case and around 20 °C for non-adiabatic case.

For validating the proposed two-dimensional dynamic model the predicted temperature profiles are also shown in Fig. 5. The calculations were performed using data listed in Table 2. The comparison proves that the model predicts very satisfactorily the complex temperature front displacement occurring in the non-adiabatic bed.

The temperature profiles in radial direction are influenced strongly by the operation mode during experiments. Experimental radial profiles are shown in Fig. 6. The measurements were carried out at fixed axial location, when the thermal wave goes through the mid of the column. Different insulation levels of the column wall are compared. In adiabatic case ($K \approx 0$, vacuum insulation jacket) a flat profile along the column radius is observed. In near adiabatic case ($K = 2.51\,\mathrm{W\,m^{-2}\,K^{-1}}$, polystyrene insulation column) significant radial temperature gradients occur only in a narrow boundary region adjacent to the wall. Completely developed radial profile through the whole section is observed in case of more intensive heat transfer to the ambience ($K = 8.62\,\mathrm{W\,m^{-2}\,K^{-1}}$, uninsulated column). A comparison between calculated and measured temperatures in case of non-adiabatic adsorption with completely developed radial profile is presented in Fig. 7. The good agreement between experimental and predicted temperature profiles in radial direction proves that the heat loss through the wall is satisfactorily interpreted by the wall external heat transfer coefficient.

The non-adiabatic conditions in respect to the adiabatic ones lead to the following effects:

- decreasing the temperature rise in the bed;
- decreasing the amplitude of the heat waves;
- decreasing the influence of the inlet and outlet.

These effects on the temperature wave lead to inverse influence on the concentration profiles because of temperature dependence on the adsorption equilibrium:

- increasing the adsorption capacity which is higher at lower temperatures;
- increasing the breakthrough time as a result of the rising of the adsorbed amount in the adsorbent particles.

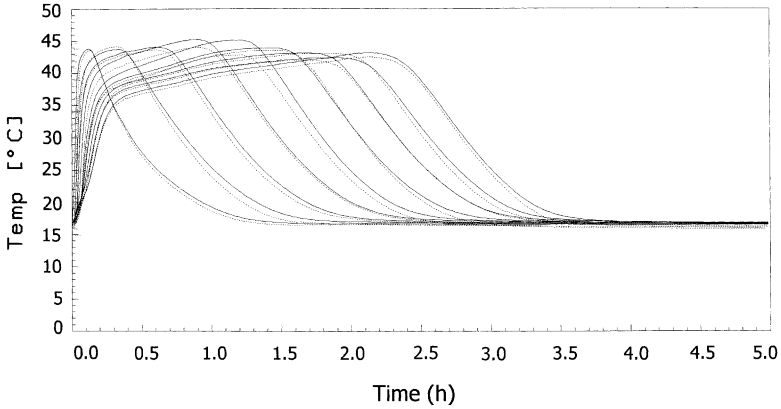

Fig. 5. Experimentally measured (—) and numerical (- - -) temperature profiles (non-adiabatic column: $K = 8.62\,\mathrm{W\,m^{-2}\,K^{-1}}$, Water on Linde 4A zeolite, $V_1 = 0.0432\,\mathrm{m\,s^{-1}}$).

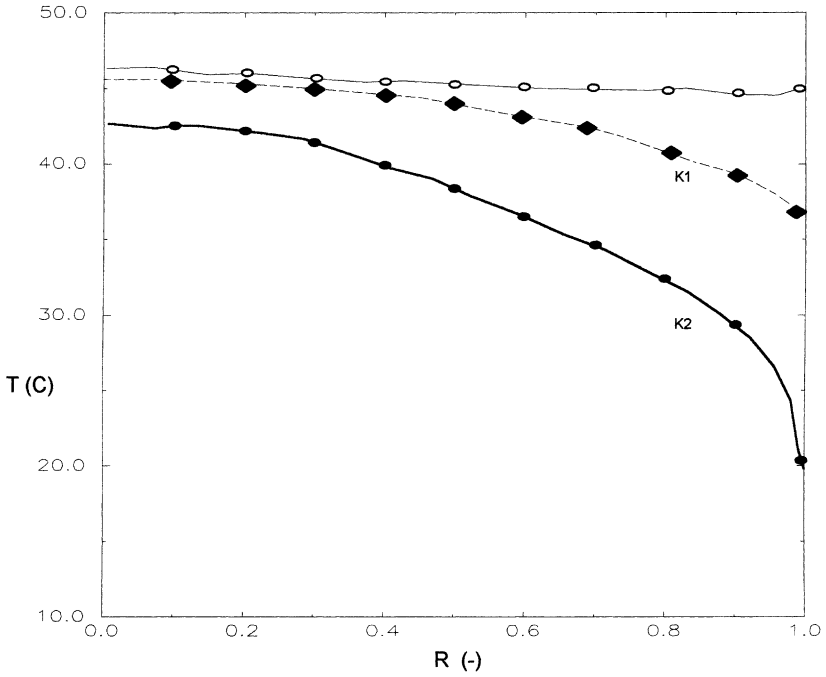

Fig. 6. Experimental radial temperature profiles with different thermal flow through the column wall adiabatic ((○) $K \approx 0$), near adiabatic ((◆) $K_1 = 2.51\,\mathrm{W\,m^{-2}\,K^{-1}}$), non-adiabatic ((●) $K_2 = 8.62\,\mathrm{W\,m^{-2}\,K^{-1}}$).

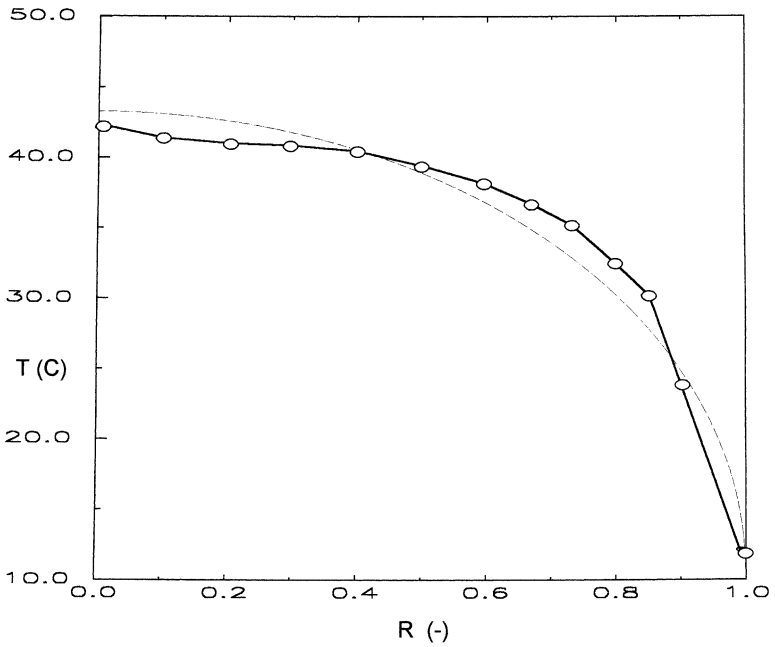

Fig. 7. Comparison of experimental (○) and numerical (- - -) radial temperature profile development for non-adiabatic operation mode.

In Fig. 8 the experimental breakthrough curves for the above-cited example in adiabatic and non-adiabatic conditions are matched with the interpreted one by the two-dimensional model. At the same time these curves are compared with the corresponding curve derived from isothermal convection–dispersion model (no heat of adsorption is considered and bed temperature is equal to the ambient). The dashed solid lines are experimentally measured data for water vapour concentration at the column outlet. The solid lines represent the model solutions for isothermal (1), non-adiabatic (2) and adiabatic (3) cases.

As expected, the assumption of isothermal adsorption (lower temperature than the realistic) provides larger breakthrough time than the measured and overestimation of the

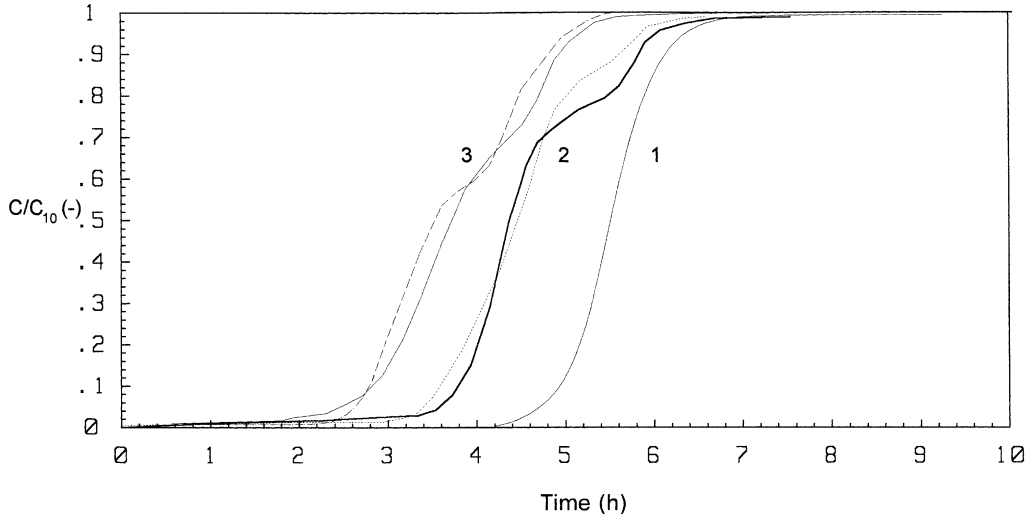

Fig. 8. Experimental and numerical breakthrough curves under different thermal conditions: (1) isothermal (—: model); (2) non-adiabatic (- - -: experiment; —: model); (3) adiabatic (-—: experiment; —: model).

adsorption capacity. On the other hand, neglecting the heat loss through the wall, we obtain lower adsorption capacity: an earlier breakthrough is observed, both experimentally and theoretically, in case of adiabatic in respect to the non-adiabatic case. Concerning the numerical solutions, good fitting of the experimental and calculated data is provided when taking into consideration heat and mass coupling dissipation effect in radial direction in the two-dimensional model, for both adiabatic and non-adiabatic conditions.

5. Discussion of experimental data

The effects of heat loss through the column wall may be explained by the relative position of the thermal and concentration front in the bed. The propagation of temperature and concentration waves in non-isothermal adsorption was investigated in particular by Pan and Basmadjian [33–36], Jacob and Tondeur [37,38], Rhee at al. [39], Sircar and Kumar [40]. The analysis is based on the theory of local equilibrium in a system in which there are no dispersive effects (no transfer resistances, as well as axial dispersion and conduction). On the basis of the derived wave equation is found that the shape and the relative velocity of the waves are determined preliminary by the equilibrium isotherm and the coupling between heat and mass balances. A dimensionless ratio is given as quantitative criterion for formation of "pure thermal wave" [35]:

$$R = \frac{q^*(T_{\max})\bar{M}/Y_{1,0}}{c_{p2}/c_{p1}} > 1.5 \qquad (22)$$

where $q^*(T_{\max})$ is the equilibrium adsorption loading at the maximum temperature. When R is significantly greater than unity, the heat is easily removed from the adsorption zone and this facilitates pure thermal wave formation. The application of this approximate analysis shows that pure thermal wave is generated in case of low feed concentration, low heat of adsorption and high equilibrium loading.

In Fig. 9 is shown the experimental breakthrough and temperature curve at the outlet of the non-adiabatic column, obtained from adsorption of acetone vapour. We performed the experiment with superficial gas velocity of $V_1 = 0.05\,\mathrm{m\,s^{-1}}$ and initial acetone concentration $C_{1,0} = 2.5 \times 10^{-5}\,\mathrm{mol\,l^{-1}}$. It is apparent that the temperature profile precedes the breakthrough curve. When the temperature reaches the peak the concentration wave appears. The effluent temperature decreases almost exponentially as the breakthrough curve rises. In case of adsorption from argon mixture the thermal capacities ratio is more important than unity because of relatively low thermal capacity of the inert carrier gas ($c_{p2} = 800\,\mathrm{J\,m^{-3}\,K^{-1}}$ and $c_{p1} = 530\,\mathrm{J\,m^{-3}\,K^{-1}}$). The low initial concentration of acetone ($Y_{1,0} = 0.0561 \times 10^{-2}$ and a respective equilibrium loading $q^* = 0.24 \times 10^{-2}$ g/g adsorbent at 283 K) leads to high values of the dimensionless ratio ($R = 3.56$). Under conditions of pure thermal wave formation and low temperature rise (about 5 K) sigmosoidal breakthrough curve and nearly constant velocity of the concentration wave are recorded.

High equilibrium loading and its small variation with temperature characterise the presented experiments for water vapour adsorption in Linde 4A zeolite ($q^* = 0.15$ g/g adsorbent at 313 K and $q^* = 0.14$ g/g at 323 K). The process is achieved under high initial water concentration ($Y_{1,0} = 5.38 \times 10^{-2}$) and lower values of the dimensionless criterion ($R = 2.34$ for non-adiabatic case and $R = 2.18$ for adiabatic case). It is apparent that if the condition (22) is not strongly fulfilled under real conditions some variation of the relative velocity of the temperature and concentration wave may occur as the process progresses.

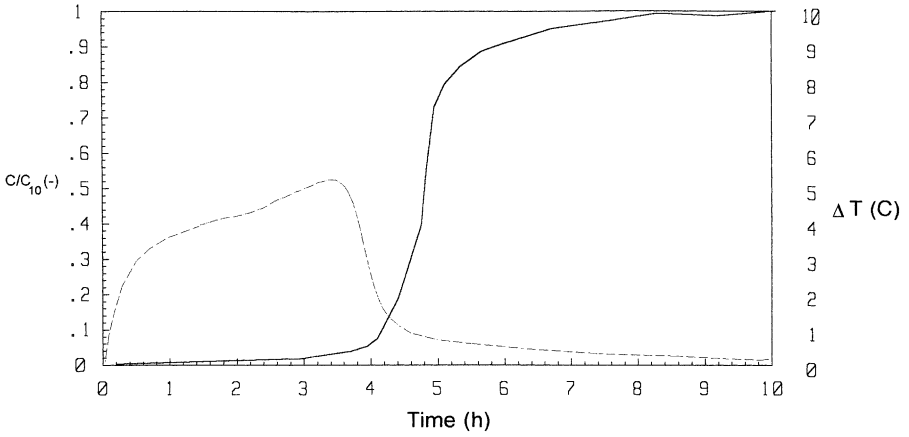

Fig. 9. Experimental temperature curves (- - -) and breakthrough (—) at the column outlet (near-adiabatic operation mode (polystyrene insulation): $K = 2.51\,\mathrm{W\,m^{-2}\,K^{-1}}$, acetone on Linde 4A zeolite, $V_1 = 0.05\,\mathrm{m\,s^{-1}}$).

For non-adiabatic case the time required for reaching T_{max} at the column exit (measured curves by thermocouple 9 in Fig. 5) coincides approximately with the breakthrough, which begins about 3 h after the concentration changes at the inlet (Fig. 8). For adiabatic conditions the length of the plateau zone expands continuously as the fronts progress through the column (Fig. 4). An overlap between the two profiles is observed: a very broad temperature flat zone is outstretched about 4 h until the curve reaches the peak (measured curves by thermocouple 9 in Fig. 4), while the breakthrough appears after 2.5 h (Fig. 8). A more complex shape of the breakthrough curves results from the combined effect of the temperature front displacement and its influence on the adsorption equilibrium. The temperature increase reduces the adsorption capacity, followed by an increase of the adsorbed amount after the passage of the temperature wave.

Although the maximum temperature achieved in the adsorbent is a function of the above-cited thermodynamic and equilibrium properties, it also depends on the adsorption dynamics. The study of Rhee et al. [38], concerning the effect of axial dispersion, shows that the profiles of the concentration wave are more strongly influenced by thermal dispersion than by mass dispersion. On the other hand, the thermal dispersion has more significant influence upon the concentration profile than upon the temperature profile. In our case short laboratory column ($L = 0.3\,\mathrm{m}$) and relatively low superficial gas velocity ($V_1 = 0.04$–$0.08\,\mathrm{m\,s^{-1}}$) are used for the experimental study. As a result relatively low Peclet numbers characterise the dispersive effects. For example, for the experimental conditions presented in Fig. 5, the dimensionless parameters take the following values:

- $D_1 = 3.4 \times 10^{-3}\,\mathrm{m^2\,s^{-1}}$; $a_1 = 6.61 \times 10^{-4}\,\mathrm{m^{-2}\,s^{-1}}$;
- in the bed: $Pe_1^{\mathrm{m}} = 3.81$, $Pe_1^{\mathrm{t}} = 19.606$;
- around the particles: $Pe_2^{\mathrm{m}} = 4.05$, $Pe_1^{\mathrm{t}} = 4.98$;
- heat loss parameter $q_{\mathrm{w}} = 1.293$ (non-adiabatic case);
- adiabatic heat rise parameter: $q_{\mathrm{a}} = 0.485$.

The lower values for the thermal dispersion lead to more important heat Peclet numbers. In the operating conditions moderate mass Peclet numbers are observed (characteristics for intermediate diffusion/convection regime), but the heat Peclet number are near to the upper limit of the regime. As a result the dispersive effects of heat affect more sensibly the characteristic velocity of the concentration front, thus increasing the dispersion of the mass transfer zone. Both thermal and mass dispersion leads to more retained adsorption wave, but they do not alter sensibly the qualitative prediction of equilibrium theory for the relative velocity of the two waves. The formation of a pure thermal wave affects the breakthrough for both adiabatic and non-adiabatic adsorption branching away from the isothermal behaviour.

6. Conclusions

It is apparent from the comparison of adiabatic, near-adiabatic and non-adiabatic behaviour that the operation mode may play an important role in adsorption dynamics, particularly for species with significant heat of adsorption and high concentration. The differences of the breakthrough curves and overall adsorption capacity can therefore be attributed to the formation of radial and axial temperature profiles.

The experimental measurements show that it is difficult to obtain uniform temperature in column section in small diameter laboratory column. Radial temperature profiles *are not* observed in perfectly insulated columns (vacuum insulation). Under near-adiabatic operation (polystyrene insulation) the temperature varies in narrow boundary region adjacent to the wall. For non-adiabatic operation significant radial profile through the whole section is recorded within

the experimental conditions. In respect to the adiabatic case, in non-adiabatic operation mode a decrease of the amplitudes of the axial temperature profiles and of the temperature peaks is detected. As a result the concentration wave is retained in respect to the thermal one under non-adiabatic conditions and the adsorption capacity is increased as a result of the lower temperatures in the adsorption zone.

For all operating modes a very complex shape of the breakthrough curve is recorded as a result of the combined effect of the temperature front displacement and its influence on adsorption equilibrium. Under non-adiabatic conditions the use of two-dimensional model taking into account the heat loss through the wall is necessary for adequate interpretation of the measurement data. As the adiabatic behaviour is approached, the observed overlap between the thermal and concentration waves leads to flattening both concentration and temperature radial profiles. The flat temperature profile in the bulk of fluid in radial direction allows the correct use of the one-dimensional model, taking into account the conduction in radial direction through the overall heat transfer coefficient.

This experimental and theoretical study confirms the necessity of preliminary experimental investigation of radial and axial temperature profiles for a particular adsorbent/gas mixture system, and arrangement of the adsorption units. Our analysis of the possible effect of the coupling between heat and mass transfer mechanisms permits the choice of the appropriate approach for process description and the correct prediction of the breakthrough curve and adsorption capacity.

References

[1] J.W. Carter, A numerical method for prediction of adiabatic adsorption in fixed beds, Trans. Inst. Chem. Engrs. 44 (1966) T253–258.

[2] A. Meyer, T.W. Weber, Non-isothermal adsorption in fixed beds, AIChE J. 13 (1966) 457–465.

[3] R.G. Lee, T.W. Weber, Non-isothermal adsorption in fixed beds, Can. J. Chem. Eng. 47 (1969) 54–59.

[4] P. Ozil, L. Bonnetain, Theoretical prediction of temperature profiles in an adsorbent fixed bed, Chem. Eng. Sci. 33 (1978) 1233–1237.

[5] L. Marcussen, Comparison of experimental and predicted breakthrough curves for adiabatic adsorption in fixed bed, Chem. Eng. Sci. 37 (1982) 299–309.

[6] H. Yoshida, D.M. Ruthven, Dynamic behaviour of an adiabatic adsorption column I, Chem. Eng. Sci. 38 (1983) 877–884.

[7] N. Raghavan, D.M. Ruthven, Dynamic behaviour of an adiabatic adsorption column II, Chem. Eng. Sci. 39 (1984) 1201–1212.

[8] H. Yoshida, T. Kataoka, D.M. Ruthven, Dynamic behaviour of an adiabatic adsorption column III, Chem. Eng. Sci. 43 (1988) 1647–1655.

[9] E. Ruckenstein, A.S. Vaidyanthan, G.R. Yongquist, Sorption by solids with bidisperse pore structures, Chem. Eng. Sci. 26 (1971) 1305–1316.

[10] A.I. Liapis, D.W.T. Rippin, The simulation of binary adsorption in activated carbon column using estimated diffusional resistance within the carbon particles derived from batch experiments, Chem. Eng. Sci. 36 (1981) 743–757.

[11] G. Nagel, G. Kluge, W. Flock, Modelling of nonisothermal multicomponent adsorption in adiabatic fixed bed. The numerical solution of the parallel diffusion model, Chem. Eng. Sci. 42 (1987) 143–153.

[12] A. Seidel, D. Gelbin, Breakthrough curves for single solutes in bed of activated carbon with a broad pore size distribution I. Mathematical models of breakthrough curves in bed of activated carbon, Chem. Eng. Sci. 41 (1986) 541–548.

[13] C.C. Lai, C.S. Tan, Approximate models for non-linear adsorption in a packed bed adsorber, AIChE J. 37 (1991) 461–465.

[14] C. Yao, C. Tien, Approximations of uptake rate of spherical adsorbent pellets and their application to batch adsorption calculations, Chem. Eng. Sci. 48 (1993) 187–199.

[15] R. Zhang, Y.A. Ritter, New approximate model for non-linear adsorption and diffusion in a single particle, Chem. Eng. Sci. 52 (1997) 3161–3172.

[16] Y.H. Ma, S.Y. Ho, Diffusion in synthetic fanjasite powder and pellets, AIChE J. 20 (1974) 279–287.

[17] M.G. Palekar, R.A. Rajadhyaksha, Sorption in zeolites: I. Sorption of single component and by many sorbate system, Chem. Eng. Sci. 40 (1985) 1085–1091.

[18] P.L. Cen, R.T. Yang, Analytic solution for adsorber breakthrough curves with bidisperse sorbents (zeolites), AIChE J. 32 (1986) 1635–1640.

[19] K. Abdallah, Ph. Grenier, Z. Sun, F. Meunier, Non-isothermal adsorption of water by synthetic NaX zeolite pellets, Chem. Eng. Sci. 43 (1988) 2633–2643.

[20] D.D. Do, P.L.J. Mayfied, A new simplified model for adsorption in a single particle, AIChE J. 33 (1987) 139–1400.

[21] H. Hu, G.N. Rao, D.D. Do, Effects of energy distribution on sorption kinetics in bidispersed particles, AIChE J. 39 (1993) 249–261.

[22] S.K. Bhatia, Transport in the bidisperse adsorbents: significance of the microscopic adsorbate flux, Chem. Eng. Sci. 52 (1997) 1377–1386.

[23] P. Keipert, M. Baerns, Determination of the intracrystalline diffusion coefficients of alkanes in H-ZSM-5 zeolite by a transient technique using the temporal-analysis-of product (TAP) reactor, Chem. Eng. Sci. 53 (1998) 3623–3634.

[24] S. Kaguei, L.W. Shemilt, N. Wakao, Models and experiments on adsorption columns with constant wall temperature—radially varying and radially lumped models, Chem. Eng. Sci. 44 (1989) 483–492.

[25] S. Farooq, D.M. Ruthven, Heat effects in adsorption column dynamics. 1. Comparison of one- and two-dimensional models, Ind. Eng. Chem. Res. 29 (1990) 1076–1084.

[26] W. Lin, S. Farooq, Ch. Tien, Estimation of overall effective coefficient of heat transfer for nonisothermal fixed bed adsorption, Chem. Eng. Sci. 54 (1999) 4031–4040.

[27] I. Park, K.S. Knaebel, Adsorption breakthrough behaviour: unusual effects and possible causes, AIChE J. 38 (1992) 660–670.

[28] D. Valenzuela, A. Myers, Adsorption Equilibrium Data Handbook, Vol. 07632, Prentice-Hall, Englewood Cliffs, NJ, 1989.

[29] C.J. Radke, J.M. Prausnitz, Thermodynamics of multi-solute adsorption from dilute liquid solutions, AIChE J. 18 (1972) 761–773.

[30] N. Wakao, T. Funazkri, Effect of fluid dispersion coefficients on particle to fluid mass transfer coefficients in packed beds, Chem. Eng. Sci. 33 (1978) 1375–1384.

[31] N. Wakao, Particle to fluid transfer coefficients and fluid diffusivities at low flow rate in packed bed, Chem. Eng. Sci. 31 (1976) 1115–1122.

[32] F. Vagliasindi, D.W. Hendrics, Wave front behaviour in adsorption reactors, J. Environ. Eng. 118 (1992) 530–550.

[33] C.Y. Pan, D. Basmadjian, An analysis of adiabatic sorption of single solute in fixed beds: pure thermal wave formation and its practical implications, Chem. Eng. Sci. 25 (1970) 1653–1664.

[34] C.Y. Pan, D. Basmadjian, An analysis of adiabatic sorption of single solute in fixed beds: equilibrium theory, Chem. Eng. Sci. 26 (1971) 45–57.

[35] D. Basmadjian, On the possibility of omitting the cooling step in thermal gas adsorption cycles, Can. J. Chem. Eng. 53 (1975) 234–238.
[36] D. Basmadjian, Rapid procedure for the prediction of fixed bed adsorber behaviour, Ind. Eng. Chem. Res. 19 (1980) 129–137.
[37] Ph. Jacob, D. Tondeur, Non-isothermal gas adsorption in fixed beds I. Non-linear Equilibrium theory and "Guillotine" effect, Chem. Eng. J. 22 (1981) 187–202.
[38] P. Jacob, D. Tondeur, Nonisothermal gas adsorption in fixed beds II. A simplistic linearized equilibrium model, Chem. Eng. J. 26 (1983) 41–58.
[39] H.K. Rhee, D. Heerdt, N.R. Amudson, An analysis of the adsorption dynamic column. II. Adiabatic adsorption of a single solute, Chem. Eng. J. 1 (1970) 279–290.
[40] S. Sircar, R. Kumar, Adsorption of a dilute adsorbate: effects of small changes in the column temperature, Ind. Eng. Chem. Res. 22 (1983) 280–287.